# Numerical Investigation of Flow and Combustion in a Single-Element $GCH_4/GOX$ Rocket Combustor: Chemistry Modeling and Turbulence-Combustion Interaction

D. Maestro,* B. Cuenot
*CERFACS, 31057 Toulouse Cedex 01, France*

L. Selle†
*IMFT, 31400 Toulouse, France*

G. Frank‡ and M. Pfitzner
*Universität der Bundeswehr München , 85577 Neubiberg, Germany*

Y. Daimon§
*Japan Aerospace Exploration Agency, Tsukuba, Ibaraki, 305-8505, Japan*

R. Keller¶ and P. Gerlinger
*University of Stuttgart, 70569 Stuttgart, Germany*

A. Chemnitz,‖ T. Sattelmayer, O. Haidn
*Technische Universität München, Munich, Bavaria, 80333, Germany*

**A sub-scale $GOx/GCH_4$ rocket combustor has been simulated by different groups using various numerical methods. The current contribution focuses on the effects of chemistry and combustion modeling on the turbulent flame shape and structure, as well as the resulting axial pressure profile and wall heat flux, for which experimental data are available. Two different kinetic schemes have been used, combined with various models for turbulence and turbulence-combustion interaction (TCI). To evaluate the impact of combustion chemistry, the schemes are first studied on canonical laminar flames and evaluated against a detailed chemical scheme. The results obtained by the different groups on the target configuration demonstrate the strong impact of the models and the consequences for pressure and wall heat flux prediction.**

## I. Introduction

Hydrocarbon fuels attract an increasing attention in the rocket engine area as potential substitutes of classical $H_2/O_2$ combustion. This is mainly due to the disadvantageous thrust-to-weight ratio of hydrogen and to the induced size of fuel tanks, which require additional cooling energy. Among the various possible hydrocarbons, methane has been found to be the most suitable candidate thanks to its characteristics: high specific impulse (higher than kerosene), favorable cooling properties, high density at common tank pressures, low pollution and low cost both in production and handling. Another significant advantage is the absence of human health risks.
In contrast with $H_2/O_2$ combustion that has been already extensively studied, there is a lack of knowledge of

*PhD student, CFD Team, 42 Avenue Gaspard Coriolis, 31057 Toulouse Cedex 01, France, maestro@cerfacs.fr
†Researcher, IMFT, Allée du Professeur Camille Soula, 31400 Toulouse, France
‡PhD student, Institute for Thermodynamics, Werner-Heisenberg-Weg 39, 85577 Neubiberg, Germany
§Researcher, Research and Development Directorate, 2-1-1 Sengen, Tsukuba, Ibaraki, Japan, Member
¶PhD student, Institute of Combustion Technology for Aerospace Engineering, Pfaffenwaldring 38-40, 70569 Stuttgart, Germany, Student Member
‖PhD student, Institute for Thermodynamics, Boltzmannstr. 15, 85748 Garching, Germany

$CH_4/O_2$ combustion at high pressure. Here CFD can be a strong assistant in the understanding of the main physical phenomena. In this context various efforts have been made. As part of a collaboration between different research teams started during the Combustion Modeling Workshop at the SFB/TRR 40 Summer Program 2015 (Technische Universität München), the flow and combustion in a single injector $GCH_4$/GOX rocket combustion chamber have been numerically simulated using different approaches. This requires special care for chemistry description and turbulence combustion interaction (TCI), which are key elements of the simulation of turbulent flames. The different approaches are here compared and analyzed to understand how chemistry and TCI contribute to the differences between the numerical solutions and to the experiment. A comparison to experimental data can be found in Roth et al.[1] The role of turbulence is studied in more detail in Chemnitz et al.[2]

First, the two chemical schemes are described and evaluated against a detailed one for canonical flame configurations. Then the different simulations are presented and compared in terms of global flame shape and flow structure. Finally, the local flame structure is analyzed in detail with respect to the different modeling approaches.

## II. Chemistry description and validation

For the combustion of methane with air or oxygen, the Gas Research Institute has developed the well-known mechanism GRI-Mech. The last version (GRI-3.0[3]) accounts for 53 species and 325 reactions. It has been validated in many configurations and over a wide range of thermodynamic conditions, where ignition delays, species concentration profiles and laminar premixed flame speed have been measured. It is considered as a reference for methane combustion. However, such kinetic schemes are difficult to use in CFD simulations because of their complexity and high computational cost. This mechanism can be used with a tabulated flamelet[4] approach, where the detailed chemical mechanism is evaluated prior to the simulation with dedicated tools, thus circumventing the computation of chemical kinetics during runtime. If the computation of chemical kinetics is included in the CFD code, chemistry must be reduced to much simpler mechanisms. These are built so as to reproduce the main features of the flame: flame speed, ignition delays and adiabatic flame temperature above all, but also flame response to stretch.[5] In the present work two different reduced mechanisms have been used and are briefly presented below.

### A. DLR skeletal mechanism[6]

A reduced skeletal mechanism has been developed specifically for space propulsion applications like that studied in the framework of the Combustion Modeling Workshop at the SFB-TR40 Summer Program 2015 by DLR (Deutsches Zentrum für Luft- und Raumfahrt), to be applied in CFD simulations of rocket combustion chambers at a pressure of 20 bar. The detailed mechanism used as input is a part of the DLR reaction database[7] and consists of 41 species (including Ar, He and $N_2$) and 298 reactions.
The reduction strategy was based on the modeling and sensitivity analysis of experimental points obtained under different operating conditions in terms of pressure, temperature and equivalence ratio. This sensitivity analysis has been implemented in the in-house code RedMaster,[8] which performed the reduction using the CHEMKIN[9] code for the chemical process and the KINALC[10] code for the calculation of sensitivity coefficients. These were used to determine and eliminate unimportant species (a species is considered unimportant if its concentration change has no significant effect on the production rate of primary species, i.e. $H_2$, $CH_4$, OH, O, CO, $O_2$, $HO_2$, H, $CO_2$, HCO, $H_2O_2$).
The result is a reduced mechanism with 24 species and 100 reactions. For the simulations performed in the present work the mechanism was further reduced to 21 species and 97 reactions, excluding Ar, He and $N_2$, since they are not relevant for the test case. The species finally included are $O_2$, O, H, $HO_2$, OH, $H_2$, $H_2O$, $CO_2$, CO, HCO, $CH_2O$, $CH_3$, $CH_3O$, $CH_4$, HCCO, $C_2H_3$, $C_2H_4$, $C_2H_5$, $CH_3O_2$, $C_2H_6$.

### B. Lu analytical mechanism[11]

Analytical mechanisms use a quasi-steady state (QSS) approximation for some species and a partial equilibrium formulation for some reactions. The quasi-steady state approach can be used when the creation rate of a species is slow compared to its consumption rate, which means that the species is very quickly consumed after being produced so that its mass can not significantly change. In this case the net rate of the species is considered equal to zero and its concentration is calculated from an analytical formulation instead of its

conservation equation, that is not solved. Partial equilibrium hypothesis is valid when both the forward and backward reaction rates of a species are fast compared to all other reactions.
Lu analytical mechanism has been derived for air/methane lean premixed combustion through the sequential application of directed relation graph (DRG),[12] sensitivity analysis and computational singular perturbation (CSP)[13] over the GRI-1.2 detailed mechanism.[14] The final skeletal mechanism contains 73 elementary reactions with 17 species, of which $CH_2$, $CH_2(S)$, HCO and $CH_2OH$ are identified as quasi-steady state (QSS) species through CSP. The remaining 13 species are fully resolved, namely, $H_2$, H, O, $O_2$, OH, $H_2O$, $HO_2$, $CH_3$, $CH_4$ , CO, $CO_2$, $CH_2O$ and $N_2$. The QSS algebraic relations are solved analytically.

It has been demonstrated (Mari[15]) how oxy-combustion of methane is quite sensitive to the number of species used in the reduced mechanism and how, if they are not sufficient, the equilibrium state of the burnt gases is not at all retrieved compared to the detailed mechanism. For this reason the comparison of the various chemical mechanisms is first performed on equilibrium calculations, followed by 1D strained counterflow diffusion flames with representative strain rate values. This is done using the CANTERA[16] software.

All calculations have been performed using the following reference values, corresponding to the experimental setup:

- Pressure: 20 bar (nominal chamber pressure)
- Inlet temperature: 275.5 K (averaged temperature of the fuel and oxidizer at inlet, weighted by their respective mass flow rates)
- Equivalence ratio: 1.5 (based on the nominal O/F ratio)

Under these conditions, the equilibrium temperature is 3290 K and the burnt gases composition, shown in table 1 is dominated by $H_2O$ and CO, which prevails over $CO_2$. It is also noticeable that $CH_4$ is completely consumed while a small quantity of $O_2$ is still present in the reaction products. Both reduced mechanisms recover the correct burnt gases state. The relative error is lower than 0.01% for the temperature and species mass fractions for the Lu mechanism. For the DLR mechanism it is slightly higher, 0.15% for the temperature and $< 4\%$ for the major species mass fractions (table 1).

**Table 1. Equilibrium values.**

| | **GRI30** | **LU** | **DLR** |
|---|---|---|---|
| Temperature [K] | 3289.11 | 3289.14 | 3283.98 |
| $O_2$ mass fraction [-] | 5.242e-3 | 5.243e-3 | 5.042e-3 |
| $CH_4$ mass fraction [-] | 4.328e-10 | 4.328e-10 | 3.153e-10 |
| $CO_2$ mass fraction [-] | 1.663e-1 | 1.663e-1 | 1.656e-1 |
| CO mass fraction [-] | 3.713e-1 | 3.713e-1 | 3.717e-1 |
| $HO_2$ mass fraction [-] | 2.196e-5 | 2.196e-5 | 2.114e-5 |
| $H_2O$ mass fraction [-] | 4.037e-1 | 4.037e-1 | 4.026e-1 |

Using the described input parameters 1D premixed flames have been computed to validate the mechanisms against the flame speed and the flame thickness. From detailed chemistry calculations these have been found to be 1.4 $m/s$ and $1.7 \times 10^{-5}$ m respectively. The flame speed is slightly under-predicted by both reduced mechanisms, with a relative error of 7% and 15% for the DLR and Lu mechanisms, respectively. The agreement on the flame thickness is excellent, with a relative error of 0.015% and 3% for the DLR and Lu mechanisms, respectively.

To represent the environment in which the flame develops in the combustion chamber, the behavior of the reduced schemes is also evaluated in conditions of strained counter-flow diffusion flames. In order to vary the strain rate applied to the flame, a series of calculations have been made with different values for the velocity of the fuel and oxidizer streams. Starting from a very low value, the strain rate is increased to a maximum of $a = 300000$ 1/s. This limit is related to the strain rate range effectively encountered in the target configuration. To evaluate this range, scalar dissipation rate along the stoichiometric surface $\chi_s = D(\partial z/\partial x_i)^2_s$, with $z$ the mixture fraction calculated according to Bilger's[17] definition, have been

extracted from the simulations in a representative area of the flow. Reminding that:

$$\chi_s = \frac{a}{\pi} exp(-2[erf^{-1}(1-2z)]^2) \tag{1}$$

where $a$ is the strain rate, and $erf$ is the error function defined as:

$$erf(\eta) = \frac{2}{\sqrt{\pi}} \int_0^\eta e^{-x^2} dx \tag{2}$$

one can retrieve the strain rate values in the numerical simulations. Applied to all simulations presented in this paper, this procedure ended up in a large spread of values. The maximum strain rate was found between 50000 1/s and 237000 1/s while the mean strain rate was found lower, between 1600 1/s and 93000 1/s. Evolutions of the maximum temperature and maximum heat release rate with the strain rate are plotted in figure 1 for the detailed and reduced mechanisms. As expected from theory, the maximum temperature decreases with increasing strain rate, as the result of faster diffusion. Conversely, the maximum heat release rate increases with increasing strain rate, until extinction suddenly occurs. For both quantities, the Lu mechanism gives results very close to the detailed mechanism. The DLR mechanism gives the exact maximum temperature, but it is less performant on the heat release rate, showing the correct trend but with smaller slope.

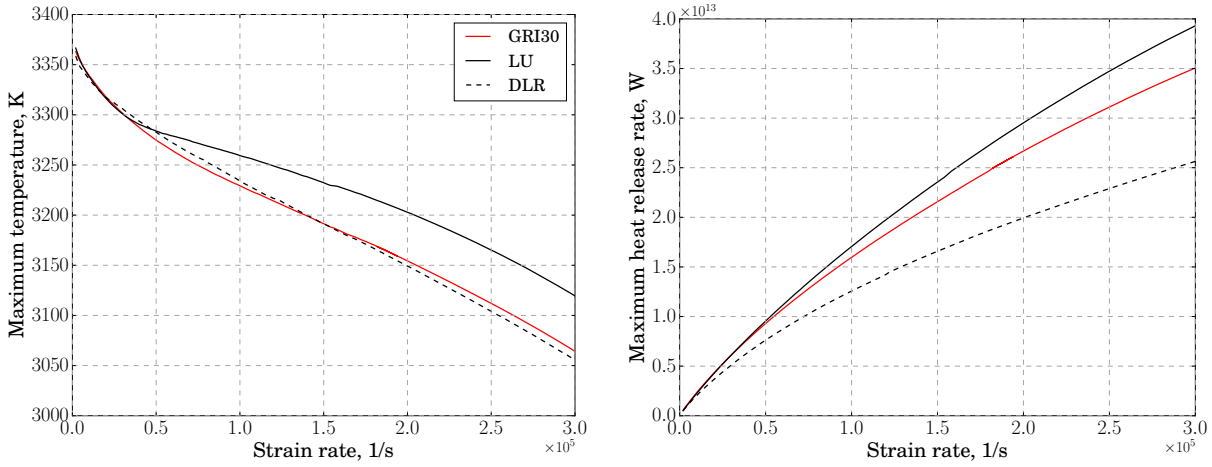


**Figure 1. Strained diffusion flames: evolution with strain rate of maximum temperature (left) and maximum heat release rate (right).**

Note that strain rates found in the numerical simulations are far from the extinction limit (evaluated for the GRI mechanism at about $a = 400000$ 1/s), and lie in the zone of fast chemistry (high Damköhler number). This indicates that for these chemical schemes, the combustion stays in the flamelet regime where a tabulated chemistry approach is well justified. Note also that the mean strain rate always stays in the range where both reduced schemes predict reasonably well the flame behavior (with the highest values of mean strain rate and using the DLR mechanism the difference in maximum of heat release rate reaches about 20 %).

The diffusion flame structures obtained with the three chemical schemes are then compared in the mixture fraction space at a representative mean strain rate value, $a = 26000$ 1/s in figure 2. The temperature and heat release rate profiles are well reproduced by both mechanisms. The temperature profile peaks near the stoichiometric value $z_s = 0.2$, where it exhibits a low curvature, indicating an already significant impact of the chemistry. This is consistent with the heat release rate profile, which extends over a relatively large range of $z$. Both reduced schemes describe well the complexity of the chemistry which results in multiple peaks of the heat release rate associated to different reactions located at different values of the mixture fraction. Note that on the rich side the temperature is slightly over-predicted by both mechanisms and especially by the Lu mechanism, due to the lack of some radicals. Note also how the maximum of heat release rate is under-predicted by the DLR mechanism, corresponding to what has been shown in figure 1.

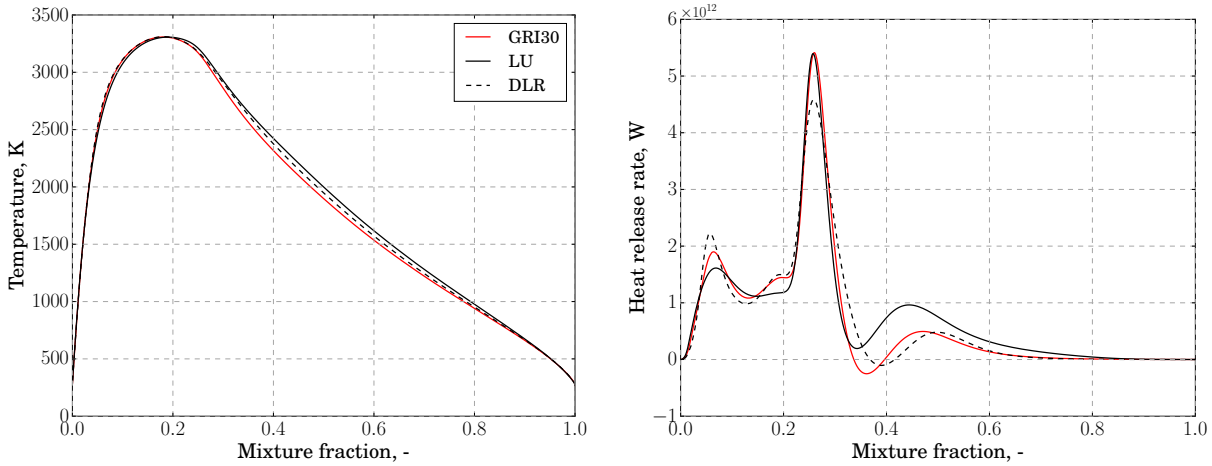


**Figure 2. Strained diffusion flame at $a = 26000$ 1/s: profile of temperature (left) and heat release rate (right).**

Mass fraction profiles for relevant species are also presented in figure 3. The following has been chosen as relevant species: the fuel, the oxydizer, a main product (CO) and a radical often used as marker of the reaction zone ($HO_2$). The reactant profiles exhibit simple monotonic behaviors, while CO peaks on the rich side and $HO_2$ shows a double peak structure. Both reduced mechanisms perfectly predict $O_2$ and CO on the oxidizer side, but show some deviation in the fuel rich region, which is to be related to the computed $CH_4$ mass fraction. Indeed in the rich side, the composition is more complex, with the presence of unburnt hydrocarbons, and therefore more sensitive to some minor radicals. Present only on the oxidizer side, the double peak of the $HO_2$ species is remarkably well reproduced by the DLR mechanism, in contrast to the Lu mechanism.

## III. Modeling of TCI

Two different strategies were used to introduce chemistry in the simulations: direct integration of chemistry and tabulated flamelets. This implies different TCI modeling approaches: direct integration of chemistry requires a resolved TCI in the case of diffusion flames, while tabulated flamelets are associated to a presumed-shape probability density function (PDF) of $z$ (typically $\beta$-PDF). In the last case, transport equations are needed to obtain the mean and rms values of $z$ which are used as parameters in the PDF. Additionally, in order to retrieve a correct heat flux, the tabulated flamelets must also be parameterized with enthalpy to account for heat losses.

## IV. Analysis of the single element $GCH_4$/GOX configuration

### A. Test case description

**Table 2. Characteristic combustion chamber and injector dimensions.**

| **Combustion chamber** | | | **Injector** | | |
|---|---|---|---|---|---|
| Chamber length | [mm] | 290 | GOx diameter | [mm] | 4 |
| Chamber width | [mm] | 12 | GOx post wall thickness | [mm] | 0.5 |
| Chamber height | [mm] | 12 | GOx post recess | [mm] | 0 |
| Throat height | [mm] | 4.8 | $GCH_4$ outer diameter | [mm] | 6 |
| Contraction ratio $A_{cc}/A_{th}$ | [-] | 2.5 | Injector area ratio $A_{GCH4}/A_{GOx}$ | [-] | 0.7 |

The experimental setup consists of a square cross section combustion chamber with a length of 290 mm and a convergent-divergent nozzle segment of 20 mm length with a rectangular throat area, see table 2. Its

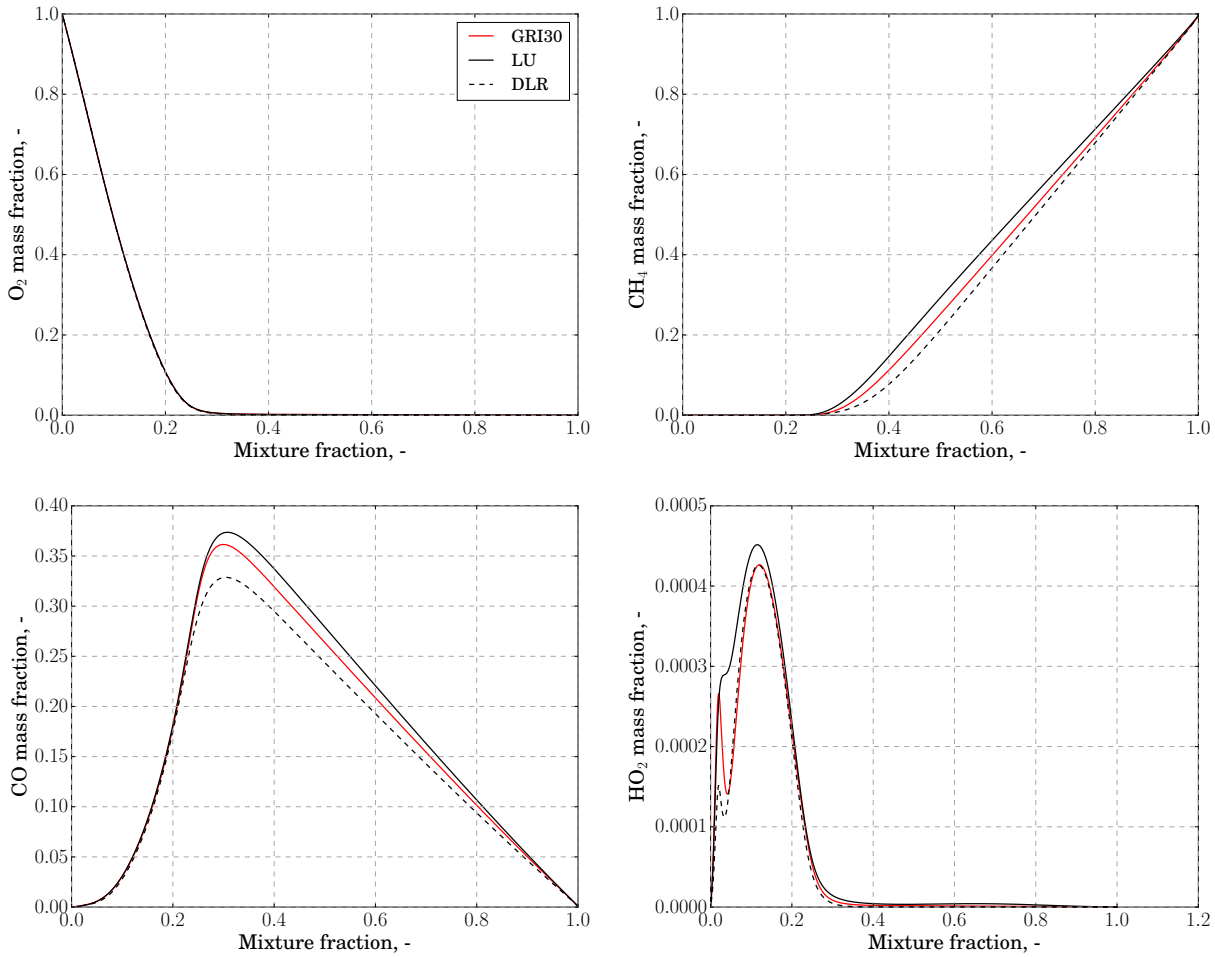


**Figure 3. Strained diffusion flame at $a = 26000$ 1/s: profile of $O_2$ (top left), $CH_4$ (top right), CO (bottom left) and $HO_2$ (bottom right).**

contraction ratio is 2.5 which roughly corresponds to operated engines. The single coaxial-type injection element is flush mounted to the chamber face-plate and provides gaseous methane at 269 K as fuel and gaseous oxygen at 278 K as oxidizer to the chamber. Within this study, the nominal operating point is characterized by an oxidizer to fuel ratio of 2.6 and a chamber pressure of 20 bar. Sonic orifices determine the inlet mass flow rates of $\dot{m}_{CH4} = 0.0017$ kg/s and $\dot{m}_{O2} = 0.0045$ kg/s, respectively. Since the chamber is capacitively cooled, the test rig is operated for a limited time per test run and thus the test case is inherently transient. Within the run time of approximately 3 s, a representative time interval is chosen to evaluate and average the measured data. Multiple pressure transducers along the axial direction of the chamber measure the combustion pressure. Thermocouples are located at different radial and axial positions in the chamber wall and therefore the assembly allows to reconstruct the wall heat flux. Detailed information concerning instrumentation, operating conditions and experimental results can be found in Celano et al.[18]

## B. Numerical approach

For a detailed description of the calculation strategies used by the different groups the reader is referred to Roth et al.[1] Here only a brief description is provided, focusing on the relevant aspects with respect to the proposed analysis. A summary is given in table 3.

Seven different simulations were performed by five groups: TUM-TD (Technische Universität München, Institute for Thermodynamics), UniBW (Universität der Bundeswehr München, which contributed with

three different simulations), JAXA (Japan Aerospace Exploration Agency), IVLR (University of Stuttgart), and CERFACS (Centre Européen de Recherche et de Formation Avancée en Calcul Scientifique). Five of these simulations are RANS (in a 3D domain for IVLR, JAXA and TUM-TD, while in a 2D domain with the same equivalent cross section of the 3D one for UniBW), while two are LES (CERFACS, on a quarter of the chamber and UniBW, on the whole chamber).
Mesh resolution obviously strongly differs between the different setups and will not be discussed in the present paper. Chamber walls are treated in all cases as isothermal, with an imposed temperature profile reconstructed from experimental data. All grids were designed to resolve the boundary layer, except for CERFACS where a law-of-the-wall approach was used.

Regarding combustion chemistry, only one 2D-RANS (UniBW) used the detailed GRI 3.0 scheme. CERFACS used the Lu mechanism. All the other simulations used the DLR reduced mechanism.
Direct integration of chemistry was applied by CERFACS in LES, where a strongly refined mesh in the flame zone was used to guarantee a resolved TCI. JAXA and IVLR also used a direct integration of chemistry in RANS, with no additional model for TCI (laminar approach). A tabulated flamelet approach has been used by UniBW, both in RANS and LES, and by TUM-TD. UniBW and TUM-TD took into account wall heat losses by solving an additional equation for the enthalpy, in order to retrieve the correct wall heat flux.

**Table 3. Summary of numerical set-ups.**

| Group | Turbulence | TCI | Walls | Chemistry |
|---|---|---|---|---|
| TUM-TD | RANS | tabulated | resolved | DLR |
| UniBW - RANS - GRI | RANS | tabulated | resolved | GRI |
| UniBW - RANS - DLR | RANS | tabulated | resolved | DLR |
| UniBW - LES | LES | tabulated | resolved | DLR |
| JAXA | RANS | direct integration | resolved | DLR |
| IVLR | RANS | direct integration | resolved | DLR |
| CERFACS | LES | direct integration | Wall law | Lu |

### C. Comparison of flow and flame general features

To check how the different modeling choices influence the result, a global comparison is first performed, looking at flame length, opening angle, combustion efficiency, maximum temperature and composition of burnt gases (see table 4). A first important conclusion is that none of the simulations reaches equilibrium at the chamber exit plane (defined as the end of the cylindrical chamber section). Deviations of the exit mean temperature from the equilibrium value vary from 12.2 % for the CERFACS simulation, which turns to be the closest to equilibrium, to a maximum of 32.7 % for both UniBW - RANS cases. Looking to the UniBW cases, it appears that the deviation from equilibrium is mostly linked to the turbulence model, as both RANS give the same deviation even with different chemistries, while LES gives a smaller deviation. The comparison to equilibrium of species mass fractions led to the same conclusions.

This deviation from equilibrium may be first related to the flame length. Most of the simulations obtained an open flame which does not close in the chamber, and in most cases even continues burning through the chamber exit. Only the TUM-TD calculation obtains a closed flame, which however closes in the immediate vicinity of the end of the combustion chamber. In both LES, the fast combustion zone ends around the half of the chamber. It is followed by a post-flame region, where slow chemistry continues to react towards equilibrium. Here pockets of $CH_4$ intermittently detach from the edges of the chamber and burn. Note that the equilibrium state changes along the chamber due to the decreasing pressure, so that the burnt gases, which do not adapt fast enough, stay out of equilibrium. To evaluate the completeness of combustion, the combustion efficiency is calculated as the ratio of the heat effectively released in the chamber to the heat that would have been released if equilibrium conditions were met at the chamber exit. Values vary from 70.9 % to 92.6 %, and tend to be higher for smaller deviation from equilibrium. A significant amount of $CH_4$ is trapped near the chamber side edges and burns only intermittently. This is due to the particular geometry

**Table 4. Summary of global features of the flame.**

| Group | Deviation from equilibrium temperature [K] | Flame angle [°] | Combustion efficiency [%] |
|---|---|---|---|
| TUM-TD | 467.6 | 2.01 | 84.8 |
| UniBW - RANS - GRI | 1067.1 | 2.33 | 71.4 |
| UniBW - RANS - DLR | 1064.9 | 2.33 | 70.9 |
| UniBW - LES | 788.9 | 4.25 | 81.1 |
| JAXA | 883.3 | 1.40 | 90.3 |
| IVLR | 521.3 | 2.40 | 92.6 |
| CERFACS | 397.9 | 10.7 | 82.8 |

of a cylindrical injector in a square-section chamber, and is found in all simulations. This applies even in the CERFACS case where the main flame closes at the walls. The chemical mechanism therefore plays a moderate role regarding the combustion efficiency, which is mainly driven by the mixing of the trapped $CH_4$ in the vicinity of the chamber edges with the bulk flow. This is also confirmed by the flame angle at the injectors exit, evaluated by means of the location of the maximum density gradient. Results show very narrow flames, with angles going from 1.4 to 2.4 degrees for most of the simulations. However, the LES performed by UniBW and CERFACS showed higher angles, respectively 4 and 10 degrees. This is again due to a stronger turbulent mixing and diffusion and is in agreement with the shorter flame and higher combustion efficiency.

### D. Comparison of flame structure

The local flame structure is classically analyzed with scatterplots of temperature vs mixture fraction. Results from the different simulations are shown in figure 4. The solution of a 1D counter-flow diffusion flame, obtained with the mechanism used in the respective simulation at the mean typical strain rate of 26000 1/s, is also plotted as a reference. The first row shows the three cases with direct integration of chemistry. They all show a classical diffusion flame structure at strain rates far from extinction. The LES simulation of CERFACS exhibits much more dispersion, due to the larger range of resolved strain rate. Note that the maximum flame temperature is effectively reached in these simulations, which may have an impact on the wall heat flux. In this first set of plots, there is no evidence of any significant effect of heat losses on the flame structure.

The second row of figure 4 shows the two simulations which use a tabulated chemistry. The UniBW case shows a very strong interaction of the flame with turbulence. The use of a PDF based TCI model is also responsible for the differences between the LES of UniBW and of CERFACS, introducing more dispersion than the resolved chemistry in the CERFACS case. This indicates a different level of mixing between the hot and cold gases, which may be under-estimated in the CERFACS LES due to the lack of sub-grid TCI, or over-estimated in the UniBW LES due to a possible over-prediction of the variance of mixture fraction. Note also the cooling of $CH_4$ in the LES of UniBW, due to heat losses effect on the flame, leading to a small secondary branch in the fuel side. In the RANS performed by TUM-TD (tabulated chemistry and PDF based TCI), contrary to the RANS of IVLR and JAXA, the PDF is here able to introduce some dispersion of the temperature profiles, with a bottom limit that is very close to the result of the RANS of UniBW (strong TCI), and an upper limit close to the RANS of IVLR and JAXA (no TCI). It is noticeable that the RANS scatterplot of TUM-TD mostly resembles the scatterplot obtained in LES by UniBW.

Scatterplots for the RANS simulations of UniBW are not shown here because there is no significant difference between the GRI and DLR mechanisms, which means that the chemistry description has little influence on the temperature field. However they confirmed that, as was already noticed in the previous section, the main effect comes from the turbulence model and the TCI one, with important differences between LES and RANS. While LES exhibits a large dispersion of strain rate, RANS flames tends to merge on a single curve. This is linked to the resolved variability of the LES, where RANS only gives a mean value. The TCI model, based on the PDF of mixture fraction, has a very strong diffusive effect on the temperature field, resulting in a significant decrease of the maximum temperature which can drop to around 2000 K in RANS, and between 2500 K and 3000 K in LES.

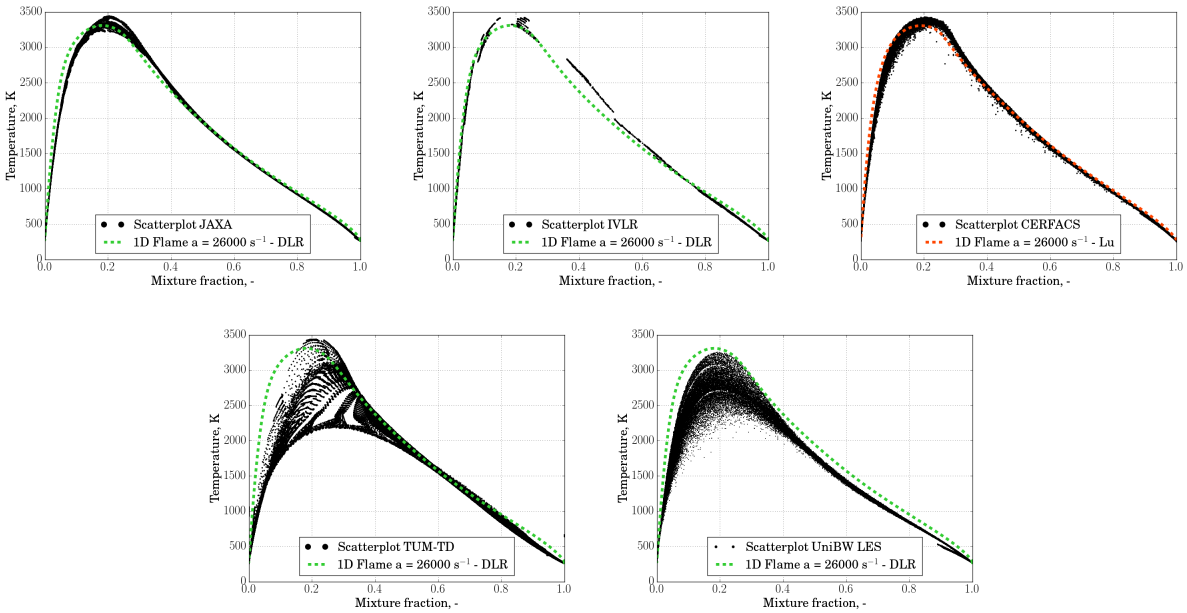


**Figure 4. Scatterplots of temperature vs mixture fraction compared to the reference 1D counter-flow diffusion flame. Top row: results from simulations with direct integration of chemistry. Bottom row: results from simulations with tabulated chemistry.**

The different behaviors of the turbulence and TCI models in the different simulations directly impact the wall heat flux, as illustrated in figure 5 by the radial profiles of the mean temperature at different axial positions ($x_1 = 50$ mm, $x_2 = 100$ mm, $x_3 = 150$ mm).

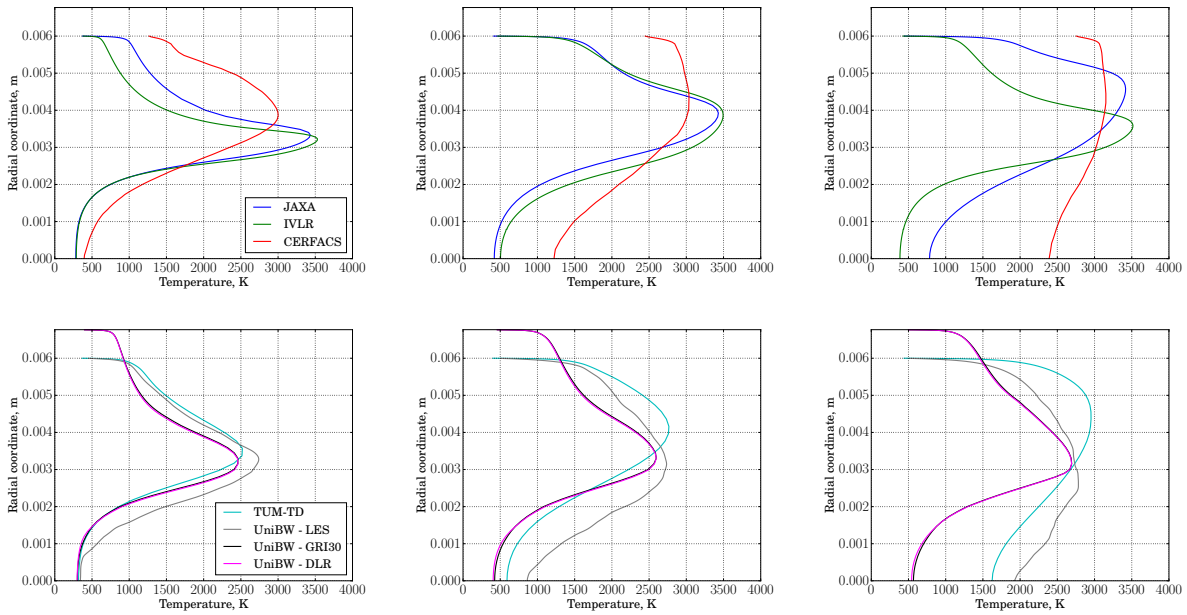


**Figure 5. Radial profiles of the mean temperature at three axial positions ($x_1 = 50$ mm, $x_2 = 100$ mm, $x_3 = 150$ mm). Top row: results from simulations with direct integration of chemistry. Bottom row: results from simulations with tabulated chemistry.**

Due to the absence of a TCI model, the JAXA and IVLR profiles exhibit the most narrow peaks, with

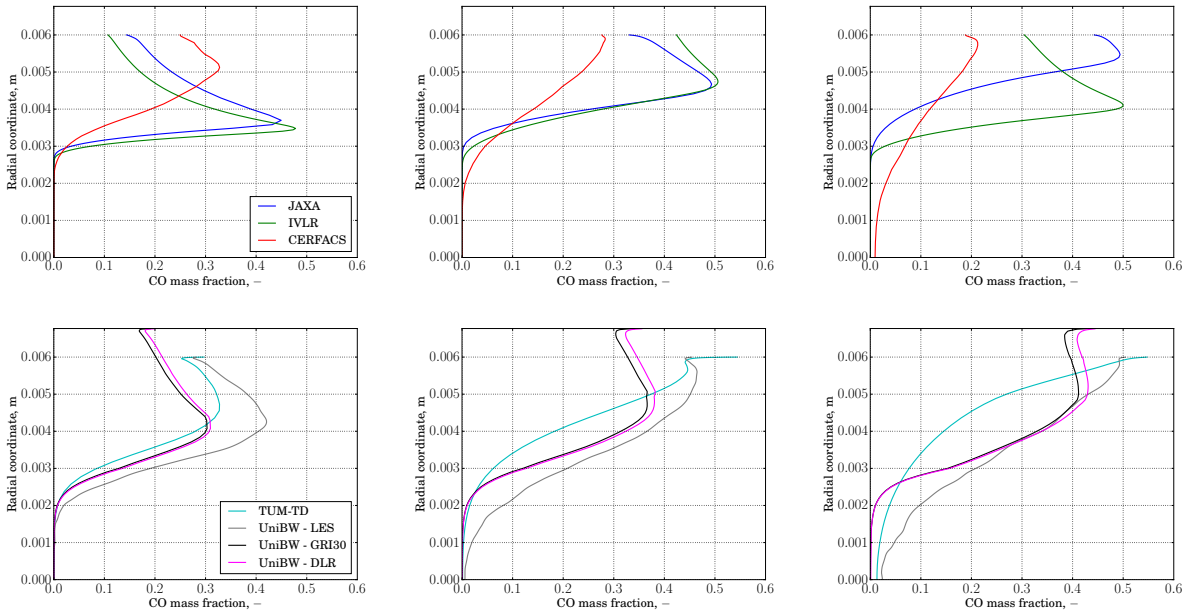


**Figure 6. Radial profiles of the mean CO mass fraction at three axial positions ($x_1 = 50$ mm, $x_2 = 100$ mm, $x_3 = 150$ mm). Top row: results from simulations with direct integration of chemistry. Bottom row: results from simulations with tabulated chemistry.**

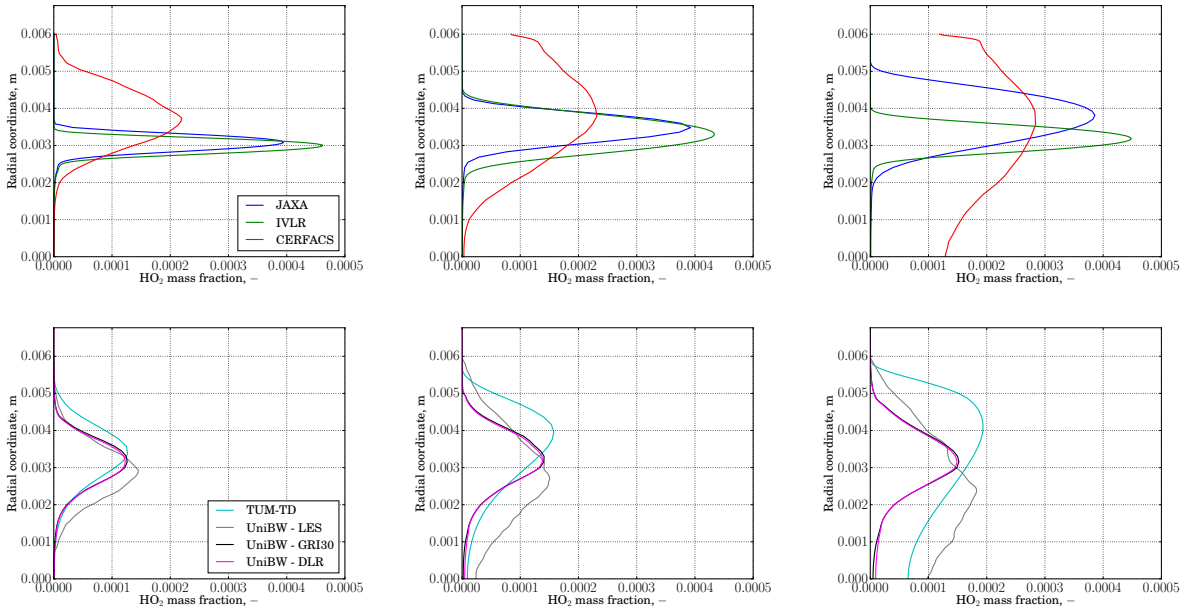


**Figure 7. Radial profiles of the mean $HO_2$ mass fraction at three axial positions ($x_1 = 50$ mm, $x_2 = 100$ mm, $x_3 = 150$ mm). Top row: results from simulations with direct integration of chemistry. Bottom row: results from simulations with tabulated chemistry.**

the highest maximum temperatures. All other cases show some effect of TCI and turbulent mixing, with a moderate reduction of the maximum mean temperature in the LES of CERFACS, and a stronger reduction in the RANS cases. All profiles decrease down to the imposed wall temperature, but with very different slopes. The homogeneity of the temperature field for the JAXA and IVLR cases, illustrated in figure 4, leads to very little mixing and the profiles resemble a laminar one, leading to a very small temperature gradient

at the wall. The RANS cases with TCI introduce more variability and therefore more mixing, leading to a reduced temperature decrease to the wall, except for the UniBW cases where, as for the JAXA and IVLR cases, no dispersion was observed in the scatter plot. Finally, both LES cases also bring significant mixing between the hot and the cold gas. Similarly to the scatterplots, the profiles of the RANS of TUM-TD are very similar to the profiles of the LES of UniBW. In the CERFACS case, the combination of a high maximum mean temperature with strong mixing leads rapidly to the presence of very hot gas close to the wall, inducing a very high temperature gradient at the wall.

The above observations are mostly linked to the turbulence and TCI models, with a very moderate impact of chemical mechanisms, which is not surprising considering that all schemes predict very well the flame temperature profile in laminar flames. The impact of combustion chemistry is more expected on the local mixture composition, illustrated by the radial profiles of some species mass fractions at the same axial positions (figures 6 and 7). As reactants and products are very well reproduced by all chemical mechanisms, similarly to the temperature, focus is made here on the intermediate species CO and $HO_2$. Both species are good markers of the deviation from equilibrium, and of low-temperature chemistry which may occur near the wall.

For both species, the JAXA and IVLR cases are very similar, and show the most marked peaks again due to the absence of a TCI model. Another common observation is the similarity of the two RANS cases of UniBW, resulting from the similarity of these species profiles in the laminar diffusion flames (figure 3) and from the tabulated chemistry, which does not allow to deviate from the laminar flame structures. These 4 cases find similar levels of CO mass fraction of about 0.3, and no $HO_2$ at the wall. Due to resolved TCI and strong turbulent mixing, the profiles obtained by the LES of CERFACS exhibit smaller and wider initial peaks that rapidly smooth out downstream. This results in a smaller CO mass fraction of about 0.2 and a non-zero mass fraction of $HO_2$ at the wall. The RANS case of TUM-TD behaves also like the RANS of UniBW, but the impact of stronger turbulent diffusion and mixing is clearly visible. Finally, the LES of UniBW is again mostly similar to the TUM-TD RANS, in particular for $HO_2$. It shows however a particular behavior for CO, with a maximum at or near the wall at all axial locations.

The presence of such species at the wall may impact the heat flux in two ways: first it may modify the local heat conductivity, and second it may sustain exothermic or endothermic chemical reactions at or near the wall. For example $HO_2$ is involved in low-activation energy reactions, which are favored near walls where the mixture is cooled down. The cooling of burnt gas near walls may also slow down the CO oxidation, which may explain the increase of CO mass fraction near the wall in the UniBW case where heat losses were included in the tabulated flamelet.

## V. Conclusions

Different simulations of a single element $GCH_4$/GOX rocket combustion chamber are compared with focus on chemistry description and TCI modeling. Results are analyzed in terms of chemical flame structure and turbulent flame development. The impact of the reaction mechanism is found to be moderate on the temperature field, which is however very sensitive to the turbulence and TCI modeling approaches. The chemical scheme however has a direct effect on the composition of the burnt gases close to the wall, which may influence the wall heat flux through the mixture heat conductivity and possible low-activation energy chemical reactions.

## Acknowledgments

Financial support has been provided by the German Research Foundation (Deutsche Forschungsgemeinschaft DFG) in the framework of the SFB/TRR 40. The authors gratefully acknowledge the Gauss Centre for Supercomputing e.V. (www.gauss-centre.eu) for funding this project by providing computing time on the GCS Supercomputer SuperMUC at Leibniz Supercomputing Centre (LRZ, http://www.lrz.de) as well as Mariella Celano, Simona Silvestri, Christoph Kirchberger and Gregor Schlieben for providing the test case.

# References


[1]Roth, C. M., Haidn, O. J., Chemnitz, A., Sattelmayer, T., Frank, G., Müller, H., Zips, J., Keller, R., Gerlinger, P., Maestro, D., Selle, L., Cuenot, B., and Riedmann, H., "Numerical Investigation of Flow and Combustion in a Single Element GCH4/Gox Rocket Combustor," *submitted for pubblication to 52nd AIAA/SAE/ASEE Joint Propulsion Conference*, 2016.

[2]Chemnitz, A., Sattelmayer, T., Roth, C. M., Haidn, O. J., Daimon, Y., Keller, R., Gerlinger, P., Zips, J., and Pfitzner, M., "Numerical Investigation of Flow and Combustion inSingle-Element GCH4/GOX Rocket Combustor: Aspects of Turbulence Modeling," *submitted for pubblication to 52nd AIAA/SAE/ASEE Joint Propulsion Conference*, 2016.

[3]Smith, G. P., Golden, D. M., Frenklach, M., Moriarty, N. W., Eiteneer, B., Goldenberg, M., Bowman, C. T., Hanson, R. K., Song, S., Gardiner Jr, W. C., et al., "GRI-Mech 3.0," *URL: http://www. me. berkeley. edu/gri_mech*, Vol. 51, 1999, pp. 55.

[4]Bray, K. and Peters, N., "Laminar flamelets in turbulent flames," *Turbulent reacting flows*, 1994, pp. 63–113.

[5]Franzelli, B. G., "Impact of the chemical description on direct numerical simulations and large eddy simulations of turbulent combustion in industrial aero-engines," 2011.

[6]Slavinskaya, N., Abbasi, M., Weinschenk, M., and Haidn, O., "Methane Skeletal Mechanism for Space Propulsion Applications," *5th International Workshop on Model Reduction in Reacting Flows (IWMRRF)*, 2015.

[7]Slavinskaya, N. A., Riedel, U., Dworkin, S. B., and Thomson, M. J., "Detailed numerical modeling of PAH formation and growth in non-premixed ethylene and ethane flames," *Combustion and Flame*, Vol. 159, No. 3, 2012, pp. 979–995.

[8]Slavinskaya, N. and Lenfers, C., "Skeletal Mechanism Production for n-decane," *2nd Int. Workshop on Model Reduction in Reacting Flow*, 2007, pp. 3–5.

[9]Kee, R. J., Rupley, F. M., and Miller, J. A., "Chemkin-II: A Fortran chemical kinetics package for the analysis of gas-phase chemical kinetics," Tech. rep., Sandia National Labs., Livermore, CA (USA), 1989.

[10]"KINALC version 1.71; see http://www.chem.leeds.ac.uk/Combustion/Combustion.html or (Turanyi et al.) http://garfield.chem.elte.hu/Combustion/Combustion.html," .

[11]Sankaran, R., Hawkes, E. R., Chen, J. H., Lu, T., and Law, C. K., "Structure of a spatially developing turbulent lean methane–air Bunsen flame," *Proceedings of the combustion institute*, Vol. 31, No. 1, 2007, pp. 1291–1298.

[12]Lu, T. and Law, C. K., "A directed relation graph method for mechanism reduction," *Proceedings of the Combustion Institute*, Vol. 30, No. 1, 2005, pp. 1333–1341.

[13]Lu, T., Ju, Y., and Law, C. K., "Complex CSP for chemistry reduction and analysis," *Combustion and Flame*, Vol. 126, No. 1, 2001, pp. 1445–1455.

[14]Frenklach, M., Wang, H., Goldenberg, M., Smith, G., and Golden, D., "GRI-MECH: An optimized detailed chemical reaction mechanism for methane combustion. Topical report, September 1992-August 1995," Tech. rep., SRI International, Menlo Park, CA (United States), 1995.

[15]Mari, R., *Influence of heat transfer on high pressure flame structure and stabilization in liquid rocket engines*, Ph.D. thesis, 2015.

[16]Goodwin, D., Moffat, H. K., and Speth, R. L., "Cantera: An object-oriented software toolkit for chemical kinetics, thermodynamics, and transport processes," *Caltech, Pasadena, CA*, 2009.

[17]Bilger, R., Stårner, S., and Kee, R., "On reduced mechanisms for methane-air combustion in nonpremixed flames," *Combustion and Flame*, Vol. 80, No. 2, 1990, pp. 135–149.

[18]Celano, M. P., Silvestri, S., Schlieben, G., Kirchberger, C., Haidn, O. J., Dawson, T., Ranjan, R., and Menon, S., "Experimental and numerical investigation of GOX-GCH4 shear-coaxial injector element," *SP-2014-2969417*, 2014.